



HAL
open science

A model coupling the liquid and gas phases for a totally wetting evaporative meniscus

Frédéric Doumenc, B. Guerrier

► **To cite this version:**

Frédéric Doumenc, B. Guerrier. A model coupling the liquid and gas phases for a totally wetting evaporative meniscus. *The European Physical Journal. Special Topics*, 2011, 197 (1), pp.281-293. 10.1140/epjst/e2011-01470-7 . hal-04387161

HAL Id: hal-04387161

<https://hal.science/hal-04387161>

Submitted on 11 Jan 2024

HAL is a multi-disciplinary open access archive for the deposit and dissemination of scientific research documents, whether they are published or not. The documents may come from teaching and research institutions in France or abroad, or from public or private research centers.

L'archive ouverte pluridisciplinaire **HAL**, est destinée au dépôt et à la diffusion de documents scientifiques de niveau recherche, publiés ou non, émanant des établissements d'enseignement et de recherche français ou étrangers, des laboratoires publics ou privés.

A model coupling the liquid and gas phases for a totally wetting evaporative meniscus

Frédéric Doumenc^{1,a} and Béatrice Guerrier¹

UPMC Univ Paris 06, Univ Paris-Sud, CNRS, lab. FAST, bat 502, Campus Univ., Orsay F-91405, France

Abstract. An hydrodynamic model has been developed to get a complete description of an evaporative meniscus in complete wetting configuration. The coupling between the liquid and gas is explicitly taken into account. Scaling laws are derived for the different domains of the meniscus and validated by numerical simulations. Results are compared with previous models of the literature that use the electrostatic analogy proposed by Deegan and co-authors to describe the evaporative flux. We show that the different approaches differ for the description of the tip of the meniscus in the domain corresponding to the decrease of the evaporative flux but lead to the same scaling for the apparent macroscopic contact angle.

1 Introduction

Evaporation of droplets or meniscus has given rise to many studies in the last years, both in terms of fundamental understanding [1] and of processing of patterned deposits (for instance [2–4]). Local description of the contact line for an evaporative droplet or meniscus is still an open question and several approaches have been recently developed to take into account the coupling between evaporation and hydrodynamics. An important distinction to be drawn concerns the gas phase surrounding the evaporating liquid. Indeed the phenomena involved are very different depending on whether the liquid is surrounded by its own vapor only [5–7] or by an inert gas. In the first configuration evaporation is driven by the departure from equilibrium at the interface while, when evaporating in an inert gas, the limiting phenomenon comes from the diffusion of the vapor in the gas [8]. In this paper we restrict the discussion to the second configuration, i.e. evaporation in an inert gas.

More specifically we focus on total wetting configurations where evaporation can modify the behavior observed for a non volatile fluid. For instance, Cazabat and co-authors [9–11] have performed numerous experiments on volatile droplets left on a substrate and observed the spreading of the droplet up to a maximum radius, followed by retraction due to the competition between wetting and evaporation. For meniscus on a moving substrate (like dip coating experiments), evaporation also changes significantly the meniscus shape when the substrate velocity is not too large (for large substrate velocities, classical Landau-Levich or Cox-Voinov models apply).

^a e-mail: doumenc@fast.u-psud.fr

Finally we restrict the study to pure fluids. Indeed, as far as complex fluids are concerned, other hydrodynamic behavior of the tip is expected due to the great change of the viscosity with solute concentration. This has been investigated in a previous study where drying of polymer solution was analyzed [12].

In this framework (evaporation in an inert gas, total wetting, pure fluid) this paper presents a numerical study and scaling laws for the different regions of the meniscus. As noticed by Deegan and co-authors [13,14], an electrostatic analogy allows to derive an estimation of the profile of the evaporative flux, as far as local description in the vicinity of the drop edge is not required. Indeed, using the electrostatic analogy, the evaporative flux is shown to diverge close to the droplet contact line. This divergence is of course not physical and one of the objective of this paper is to evaluate the validity of that model by comparing it with a more sophisticated approach including the coupling between the gas phase and the liquid. We thus compare our results to different models developed in the literature [9,15,16].

2 Problem formulation

2.1 Model equations

The geometry considered here corresponds to the capillary rise of a volatile fluid between two parallel plates immersed in an infinite reservoir. We consider a stationary configuration where the meniscus is motionless. The temperature is assumed uniform (isothermal problem). Coupled mass transfers in the liquid and in the gas phases are taken into account. Drying takes place in air at atmospheric pressure, local thermodynamic equilibrium is assumed at the interface and the evaporation is limited by the solvent vapor transfer into stagnant air (1.5-sided model).

In the liquid phase the velocity field is assumed quasi-parallel to the substrate (lubrication approximation) with no-slip at the substrate and zero tangential stress at the free surface. The direction of the flow is noted \mathbf{x} , the axis normal to the substrate is \mathbf{z} . Gravity is neglected.

This model is very close to the one developed previously in the same geometry for a binary solution on a moving substrate [12], or to the one used by Eggers and Pismen for a drop of volatile liquid [15].

With the above-mentioned approximations Stokes equations lead to the standard result [5]:

$$Q(x, t) = \frac{h^3}{3\eta} \frac{\partial}{\partial x} \left(\sigma \frac{\partial^2 h}{\partial x^2} + \Pi_d \right) \quad (1)$$

where h is the liquid height, η the dynamic viscosity, σ the surface tension and Π_d the disjoining pressure. To model total wetting we use a long-range stabilizing Van der Waals disjoining pressure $\Pi_d = A/(6\pi h^3)$ with the Hamaker constant $A > 0$. $Q(x, t)$ is the liquid volumic flux (by unit of width) at abscissa x and time t over a cross section normal to \mathbf{x} ,

$$Q(x, t) = \int_0^{h(x)} u(x, z) dz \quad (2)$$

where $u(x, z)$ is the velocity component in the \mathbf{x} direction.

The mass conservation reads:

$$\frac{\partial h}{\partial t} + \frac{\partial Q}{\partial x} = -v_{ev}(x, t) \quad (3)$$

where $v_{ev}(x, t)$ is the local evaporation velocity (positive for evaporation).

The boundary conditions are the following: at $x = 0$ we impose the liquid height h_0 and the curvature C_0 . If one performs an analogy with previous capillary rise experiments [18], C_0 is the curvature of a static meniscus, deduced from the gap d between the plates: $C_0 = 2/d$, with $d = 1\text{mm}$. The lubrication theory is valid if the free surface slope is much lower than 1, which is true if h_0 is small enough.

With the geometric assumptions of the model, we define a length L_{st} used in the following as the order of magnitude of the meniscus size: considering a parabolic meniscus (constant curvature C_0 and small slope approximation) of height h_0 at $x = 0$, it intercepts the substrate at $x = L_{st}$ with zero contact angle. A simple derivation gives $L_{st} = \sqrt{2h_0/C_0}$.

Spatial derivatives of h in equation 1 being of fourth order, two boundary conditions are also needed at $x = W$. These conditions far from the bulk are given in equation 5 (as far as the length of the simulation box is large enough, we have checked that the choice of the outlet conditions does not affect the results).

$$\text{at } x = 0 : \quad h = h_0 \qquad \frac{\partial^2 h}{\partial x^2} = C_0 \qquad (4)$$

$$\text{at } x = W : \quad \frac{\partial h}{\partial x} = 0 \qquad \frac{\partial^2 h}{\partial x^2} = 0 \qquad (5)$$

The local evaporation velocity in equation 3 is determined by solving a diffusion problem in the gas phase, in a domain of length W and height H (for process with a forced air flow above the free surface, H would roughly correspond to the boundary layer thickness). Since H is much larger than h_0 , we assume a rectangular domain for the gas phase. This means that liquid thickness variations are neglected when computing mass transfer in the gas phase. The bottom boundary of this domain corresponding to the liquid-gas interface is then: $z = 0$ and $0 < x < W$. The diffusion equation in the gas phase reads:

$$\frac{\partial c_g}{\partial t} = D_g \left(\frac{\partial^2 c_g}{\partial x^2} + \frac{\partial^2 c_g}{\partial z^2} \right) \quad \text{for } 0 < x < W \quad \text{and} \quad 0 < z < H \qquad (6)$$

where c_g is the solvent vapor concentration in the air. The vertical walls are assumed impermeable. At the top a Dirichlet condition is imposed, with solvent vapor concentration equal to c_{gH} . Then we get the following boundary conditions for the gas domain:

$$\frac{\partial c_g}{\partial x} = 0 \qquad \text{for } (x = 0 \text{ or } x = W) \quad \text{and} \quad 0 < z < H \qquad (7)$$

$$c_g = c_{gH} \qquad \text{for } 0 \leq x \leq W \quad \text{and} \quad z = H \qquad (8)$$

The last boundary condition corresponds to the coupling between the liquid and the gas phases and is achieved by writing the mass flux conservation and the local thermodynamic equilibrium at the interface:

$$\rho v_{ev} = -D_g \frac{\partial c_g}{\partial z} \qquad \text{for } 0 \leq x \leq W \quad \text{and} \quad z = 0 \qquad (9)$$

$$c_g = c_{gs0} \exp\left[-\frac{\bar{v}_s}{RT} \left(\sigma \frac{\partial^2 h}{\partial x^2} + \Pi_d \right)\right] \qquad \text{for } 0 \leq x \leq W \quad \text{and} \quad z = 0 \qquad (10)$$

with $c_{gs0} = \frac{M_s}{RT} P_{vs0}(T)$. ρ is the liquid solvent density, M_s the liquid molar mass, R the ideal gas constant, T the temperature, P_{vs0} the bulk saturated vapor pressure of the fluid, and \bar{v}_s its molar volume. As already said, evaporation cooling effect is

disregarded so the temperature T is assumed uniform in the whole system, and equal to the surrounding temperature.

This paper focuses on the steady state and we use as initial conditions the result of a previous calculus for a close configuration. It has been checked that the choice of the initial conditions has no effect on the steady state result.

The above set of equations (1 to 10) is solved numerically by finite differences, using a pure implicit scheme of order 1 in time and 2 in space. At each time step equations are solved iteratively in the liquid and in the gas, until convergence is achieved. The discretization of equations in the liquid (1 to 5 and 9) leads to a set of nonlinear algebraic equations, solved by Newton-Raphson algorithm. An adaptive mesh is implemented, in order to refine the mesh in the region of high evaporative flux. In the gas phase, the set of algebraic equations resulting from discretization of equations 6 to 8 and 10 is linear, and solved by Successive Over-Relaxation method (SOR). A specific software has been written in Fortran, and most of the computations have been performed on iDataPlex IBM clusters. Computational times vary from a few hours to several weeks for high evaporative flux.

3 Results

3.1 Local description

We first present a detailed analysis of the meniscus shape, the liquid flow, the local evaporative flux and the concentration field in the gas for a reference configuration corresponding to the following data: the box dimensions are $W = 1mm$ and $H = 3mm$, the boundary conditions are $h_0 = 0.1mm$, $C_0 = 2mm^{-1}$ and $c_{gH} = 0$. Physical properties are close to properties of toluene at $25^{\circ}C$: $\rho = 900kg.m^{-3}$, $\sigma = 30mN.m^{-1}$, $M_s = 92.14g.mol^{-1}$, $\eta = 0.55mPa.s$. Vapor diffusivity in the air is $D_g = 8.6 \times 10^{-6}m^2.s^{-1}$ and the saturated vapor pressure is given by Antoine equation: $\log(P_{vs0}) = a_1 - a_2/(T + a_3)$, with $a_1 = 9.0782$, $a_2 = 1343.9$, $a_3 = -53.77$, P_{vs0} in Pascal and T in Kelvin. The Hamaker constant is $A = 10^{-19}J$.

The profile of the meniscus is given in figure 1(a). From the observation of the meniscus slope (figure 1(b)), the liquid pressure (figure 1(c)) and the evaporation rate (figure 1(e)), we can split the meniscus into four characteristic domains, with the corresponding boundaries x_1 to x_4 :

- Bulk region ($0 \leq x \leq x_1$). In the bulk the slope $\partial h/\partial x$ varies linearly with x (i.e. quasi constant curvature approximately equal to C_0) and the meniscus profile is then parabolic. The first boundary x_1 corresponds to a significant change in the meniscus curvature, arbitrarily set to 10%. In the following we call macroscopic angle the value of the slope at $x = x_1$.
- Capillary domain ($x_1 \leq x \leq x_2$). This domain is characterized by a strong increase of the curvature. The pressure in the liquid film is dominated by the capillary term. The boundary x_2 corresponds to equality between the capillary pressure and disjoining pressure.
- Precursor film ($x_2 \leq x \leq x_4$). In this domain the disjoining pressure dominates over the capillary pressure and the evaporative flux is non negligible. It can be split into two sub-domains: a region of increasing evaporative flux ($x_2 \leq x \leq x_3$) followed by a region of decreasing evaporative flux ($x_3 \leq x \leq x_4$). The evaporative flux is thus maximum for $x = x_3$.
- Adsorbed film ($x > x_4$). Finally the meniscus ends by a film of nanometric thickness where the evaporative flux and liquid flow are almost zero. We call x_4 the abscissa where the evaporative flux is less than 3% of its maximum value. Evaporation is assumed negligible for $x > x_4$.

The four boundaries characterizing the different domains of the meniscus (based on order of magnitude arguments) are reported on all the figures describing the local behavior of the meniscus. The local shape of the meniscus results from the coupling with the 2D vapor concentration field in the gas phase. Indeed a strong deformation of isoconcentration lines in the gas phase is observed at the meniscus tip, as shown in figure 1(d).

3.2 Evaporative flux

In the following we often argue about orders of magnitude. In that case the numerical prefactors are disregarded.

The total evaporative flux I and the mean evaporation rate \bar{v}_{ev} read:

$$I = \int_0^W v_{ev}(x)dx \quad \text{and} \quad \bar{v}_{ev} = \frac{1}{x_4} \int_0^W v_{ev}(x)dx \simeq \frac{1}{L_{st}} \int_0^W v_{ev}(x)dx \quad (11)$$

For $x_4 = W$ (length of the box), the vapor transfer in the gas is 1D and the total evaporative flux simply reads

$$I_{1D} = \frac{D_g}{\rho H} (c_{gs0} - c_{gH})W$$

For $x_4 < W$ and $W \ll H$, the isovalues of the vapor concentration are similar to those of the 1D configuration in most part of the box and the total evaporative flux is then almost the same (cf [12] for more details). Then we get the following scalings

$$\bar{v}_{ev} \sim v_{ev}^{sc} \quad \text{with} \quad v_{ev}^{sc} \equiv \frac{D_g}{\rho H} (c_{gs0} - c_{gH}) \frac{W}{L_{st}} \quad (12)$$

This scaling is still relevant in our case where $H = 3W$, as shown in figure B.1(a). For a droplet in a semi-infinite medium, one should choose $H \sim W \sim L_{st} \sim R$, with R the droplet radius.

As already noticed in the introduction, Deegan and co-authors use an electrostatic analogy to get an estimation of the profile of the evaporative flux for a droplet, which scales as $1/\sqrt{x_{div} - x}$ in the vicinity of the droplet's edge and diverges at the droplet's edge x_{div} . Several authors use this expression to model the evaporation of droplets or to compute macroscopic contact angle. It is then interesting to compare the evaporative flux deduced from numerical simulation to this law. In this aim of view, the evaporative rate deduced from the above model is approximated by $w_{ev}(x) = J_0/\sqrt{x_{div} - x}$. The two parameters J_0 and x_{div} are fitted to get $w_{ev}(x) \simeq v_{ev}(x)$ for $x \lesssim x_3$ (i.e. before the peak of the evaporative flux). For the reference configuration we get $J_0 = 9.78 \cdot 10^{-9} m^{3/2} s^{-1}$ and $x_{div} = 293.56 \mu m$. The two evaporative fluxes $v_{ev}(x)$ (numerical simulation) and $w_{ev}(x)$ (electrostatic analogy) are compared in figure 1(e) for the reference case. As can be seen the approximation is consistent with our model for $x \lesssim x_3$. At the very end of the meniscus evaporation fades away and then the electrostatic analogy does not hold anymore.

Figure 1(f) shows the integrals of the evaporative flux from the end of the box ($x = W$) for the two expressions $v_{ev}(x)$ and $w_{ev}(x)$, that is:

$$I(x) = \int_x^W v_{ev}(x)dx \quad \text{and} \quad I_w(x) = \int_x^W w_{ev}(x)dx$$

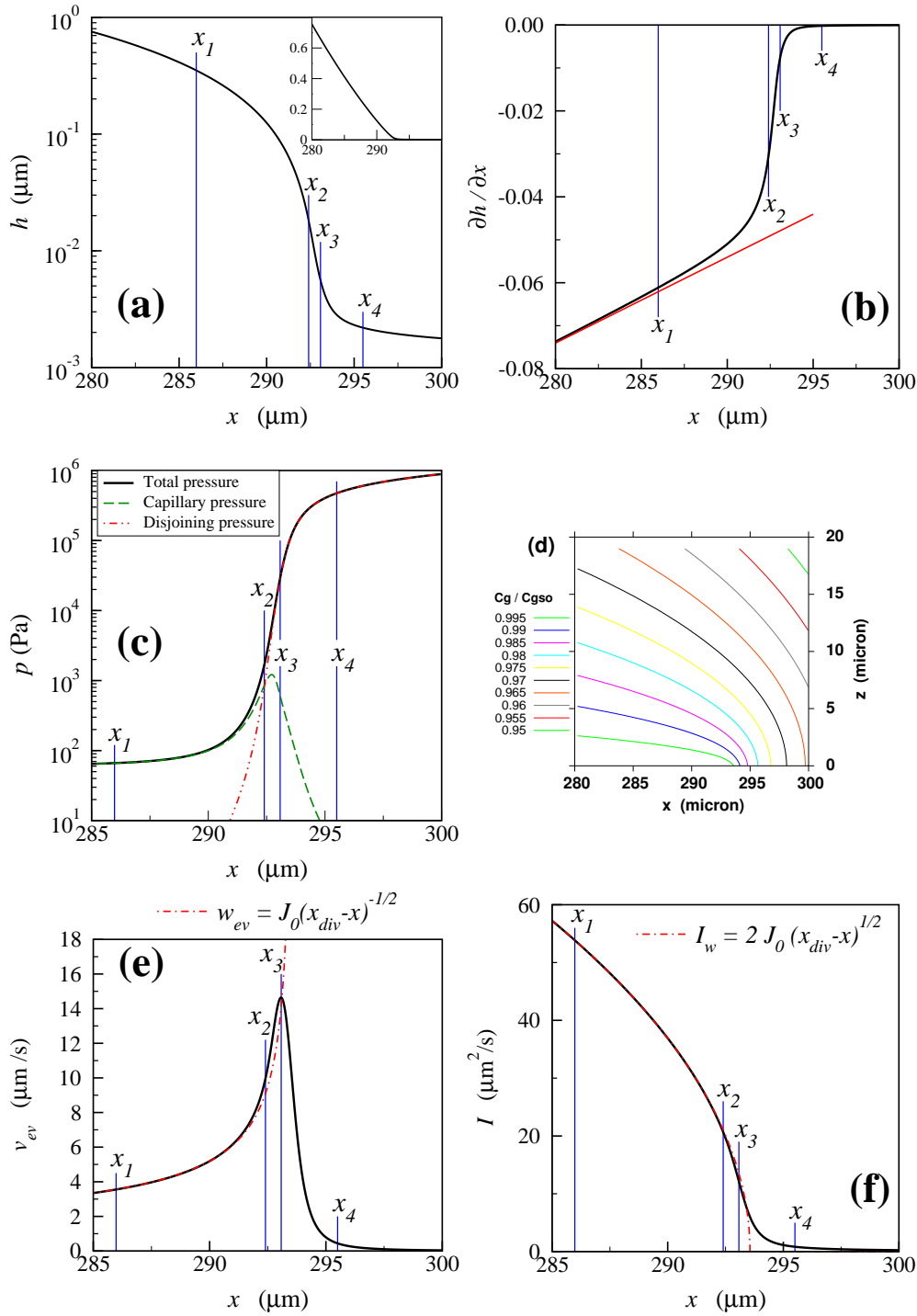


Fig. 1. Meniscus structure, (a) Liquid height (semilogarithmic scale, linear scale in the insert), (b) Slope, (c) Liquid pressure, (d) Normalized concentration isovalues in the gas phase c_g/c_{g0} , (e) Evaporation rate, (f) Integral of evaporation rate.

Since the box is large enough to get $v_{ev}(W) \simeq 0$, since the problem is stationary and the substrate is motionless, mass conservation implies the equality of $I(x)$ with the hydrodynamic flux $Q(x)$. On the other hand it can be seen that for $x \lesssim x_3$, i.e. before the peak of the evaporative flux, the two integrals $I(x)$ and $I_w(x)$ are very close (figure 1(f)), which means that the hydrodynamic flux that goes through the film for $x \lesssim x_3$ is the same for the two representations of the evaporative flux.

We are now going to derive the scaling laws for the maximum of the evaporative flux v_{ev}^{max} and the length $(x_4 - x_3)$ corresponding to the decrease of the evaporative flux. For $x \sim x_3$ an estimation of the integrals is derived from the two models.

The flux is maximum for $x = x_3$ and varies regularly until $x \simeq x_4$, then we can write

$$Q(x_3) = I(x_3) \sim (x_4 - x_3) v_{ev}^{max} \quad \text{with} \quad v_{ev}^{max} = v_{ev}(x_3) \quad (13)$$

$I_w(x_3)$ can be deduced directly from the analytical expression of $w_{ev}(x)$:

$$I_w(x_3) \sim J_0 \sqrt{x_{div} - x_3}$$

The numerical simulations suggest that $I(x_3) \sim I_w(x_3)$ and $v_{ev}(x_3) \sim w_{ev}(x_3)$. Then we easily deduce the following relation:

$$(x_4 - x_3) \sim (x_{div} - x_3) \quad (14)$$

At $x = x_3$ the capillary pressure is much lower than the disjoining pressure and can be disregarded so that equation 1 reads:

$$Q(x_3) \sim \frac{A}{\eta h} \frac{\partial h}{\partial x} \quad (15)$$

In this domain the film is thin enough for the disjoining pressure to affect the saturated vapor pressure so that the evaporative flux and film height are strongly coupled. We then assume that the evaporative flux and film height decrease of one order of magnitude on the same length $(x_4 - x_3)$. Using $I(0) \sim I_w(0)$ and equations 13, 14 and 15 lead to the following scaling:

$$(x_4 - x_3) \sim (x_{div} - x_3) \sim \xi \quad \text{with} \quad \xi \equiv \left(\frac{A}{\eta v_{ev}^{sc} \sqrt{L_{st}}} \right)^{2/3} \quad (16)$$

At last, approximating the total length of the meniscus x_4 by L_{st} , we easily get:

$$v_{ev}^{max} \sim v_{ev}^{sc} \sqrt{L_{st}/\xi} \quad (17)$$

Equations 16 and 17 are the desired scalings. It is worthwhile to notice that the two lengths corresponding to the tip of the meniscus, the real one $(x_4 - x_3)$ and the fictive one $(x_{div} - x_3)$, both scale as ξ .

3.3 Scaling laws of local slopes and thicknesses

This section is dedicated to the derivation of the scaling laws allowing the local description of the meniscus for the different domains described in section 3.1. Moving back towards the bulk we express in the vicinity of $x = x_2$ the balance between the effect of the capillary pressure, the disjoining pressure and the evaporation. Using the

Table 1. Scaling laws.

$(x_2 - x_1) \sim a^{1/3}/C_0^{2/3}$	$h_1 \sim a^{5/6}/(\xi^{1/2}C_0^{2/3})$	$\theta_1 \sim (a/\xi)^{1/2}$
$(x_4 - x_2) \sim \xi$	$h_2 \sim (a\xi)^{1/2}$	$\theta_2 \sim (a/\xi)^{1/2}$
$(x_4 - x_3) \sim \xi$	$h_3 \sim \lambda^{2/3}\xi^{1/3}$	$\theta_3 \sim (\lambda/\xi)^{2/3}$

same arguments than in the previous section, the balance between the flux induced by the disjoining pressure and the evaporation leads to the same scaling, i.e.

$$(x_4 - x_2) \sim \xi$$

At $x = x_2$ the pressures are equal so that we get

$$\frac{A}{h^3} \sim \sigma \frac{\partial^2 h}{\partial x^2}$$

Assuming that the height and slope decrease of at least one order of magnitude between x_2 and x_4 (cf figure 1), we obtain

$$h_2^4 \sim \xi^2 A / \sigma \quad \text{and} \quad \theta_2 \sim h_2 / \xi$$

that is

$$h_2 \sim \sqrt{\xi a} \quad \text{and} \quad \theta_2 \sim \sqrt{a/\xi} \quad (18)$$

with $a \equiv \sqrt{A/\sigma}$, $h_2 \equiv h(x_2)$ and θ_2 the local slope at $x = x_2$. Using the same approach, scaling laws have been derived for the film heights, $h_i \equiv h(x_i)$, the domain lengths and the local slopes in the different regions of the meniscus. They are summarized in Table 1 and detailed in the appendix A. For h_1 and θ_1 they are derived from the approximated expression of the flux, that is $w_{ev}(x)$. In the region such that $x_3 \lesssim x \lesssim x_4$, the local description of the coupling between the liquid and the gas must be taken into account to get h_3 and θ_3 .

This analysis shows that the relevant length scales involved in the problem are the following:

$$\lambda \equiv \frac{\bar{v}_s}{RT} \sqrt{\eta P_{vs0} D_g} \quad , \quad a \equiv \sqrt{\frac{A}{\sigma}} \quad , \quad \xi \equiv \left(\frac{A}{\eta v_{ev}^{sc} \sqrt{L_{st}}} \right)^{2/3} \quad (19)$$

λ and a are microscopic lengths which depend only on the fluid physical properties. For most of the common volatile fluids at room temperature, $\lambda \sim 0.1nm$ and $a \sim 1nm$. Only the characteristic length ξ depends on the evaporative flux. In that study, it has been varied from 0.1 to $1000\mu m$. The geometry of the problem appears through the length $L_{st} = \sqrt{2h_0/C_0}$.

In order to confirm the above scalings and their validity domain, simulations were performed for a large range of parameters, i.e. the humidity, temperature and system properties. The parameters of the simulations are resumed in Table 2. Results of numerical simulations compare very well with scaling laws, as shown in figures 2 and B.1. The limit of validity of the scalings can clearly be observed on the figures and are detailed in next section.

3.4 Validity domain of the scaling laws

A first limitation of the above description is obtained when the peak of the evaporative flux occurs in the domain where the capillary pressure is dominant, i.e. when x_3

Table 2. Parameters used in the simulations. Only the parameters different from the reference case are noted. Symbols are used in figures 2 and B.1. (*): P_{vs0} computed from Antoine’s law.

Serie	Symbol	T $^{\circ}C$	c_{gH}/c_{gs0}	L_{st} μm	D_g $mm^2.s^{-1}$	P_{vs0} Pa	A J	η $mPa.s$	σ $mN.m^{-1}$
Ref. case		25	0	316	8.6	(*)	10^{-19}	0.55	30
#1	\triangle		[0; 0.99]						
#2	∇		[0; 0.99]				10^{-20}		
#3	\triangleleft		0.5		[3; 100]				
#4	\triangleright	[-10; 52]							
#5	\diamond					[1; 3792]			
#6	+		0.9					[0.1; 550]	
#7	\times		0.5					[0.1; 55]	
#8	*	6.85						[0.1; 55]	
#9	\circ		0.5						[10, 100]
#10	*	6.85							[10, 100]
#11	\square		0.5	[100; 316]					

becomes smaller than x_2 . Indeed the arguments used to derive ξ neglect the capillary pressure which is no more valid in this configuration. The first limit of validity is then given by the condition $h_2 \gtrsim h_3$, that is

$$\xi^{1/6} a^{1/2} \lambda^{-2/3} \gtrsim 1$$

However this must be viewed as a theoretical limit. Indeed, in realistic configurations of evaporation in an inert gas, it seems that no real liquid can go beyond this limit (even if the prefactors are taken into account).

The other limitation corresponds to the violation of the condition $h_2 \lesssim h_1$, which leads to:

$$\xi a^{-1/3} C_0^{2/3} \lesssim 1$$

Beyond this limit evaporation turns to be negligible and the meniscus profile tends to the classical solution corresponding to thermodynamic equilibrium for a non volatile fluid. From pressure equality between the film and the bulk domain, we get $h_1 \sim h_2 \sim a^{2/3}/C_0^{1/3}$.

4 Comparison with other models

In this last section our results are compared to the models proposed by Cazabat and co-authors [9–11] on one hand, and Pham and co-authors [16] on the other hand. The first model is dedicated to droplet evaporation, while the later addresses the problem of an evaporating wedge, with zero curvature far from the contact line. Total wetting is assumed in both cases, and the evaporative flux is described by Deegan’s electrostatic analogy. The main difference in the two approaches lies in the treatment of the precursor film.

- Cazabat et al [10] assume that close to the droplet edge, the leading terms in equations 1 and 3 are the capillary and the disjoining pressures, and then neglect advection and evaporation in that region. This leads to a tip profile which scales like \sqrt{ax} . The crossover to the macroscopic region with contact angle θ is found to take place at a distance of order $a\theta^{-2}$, where the disjoining pressure turns to be negligible, and the evaporation rate reaches its maximum value.

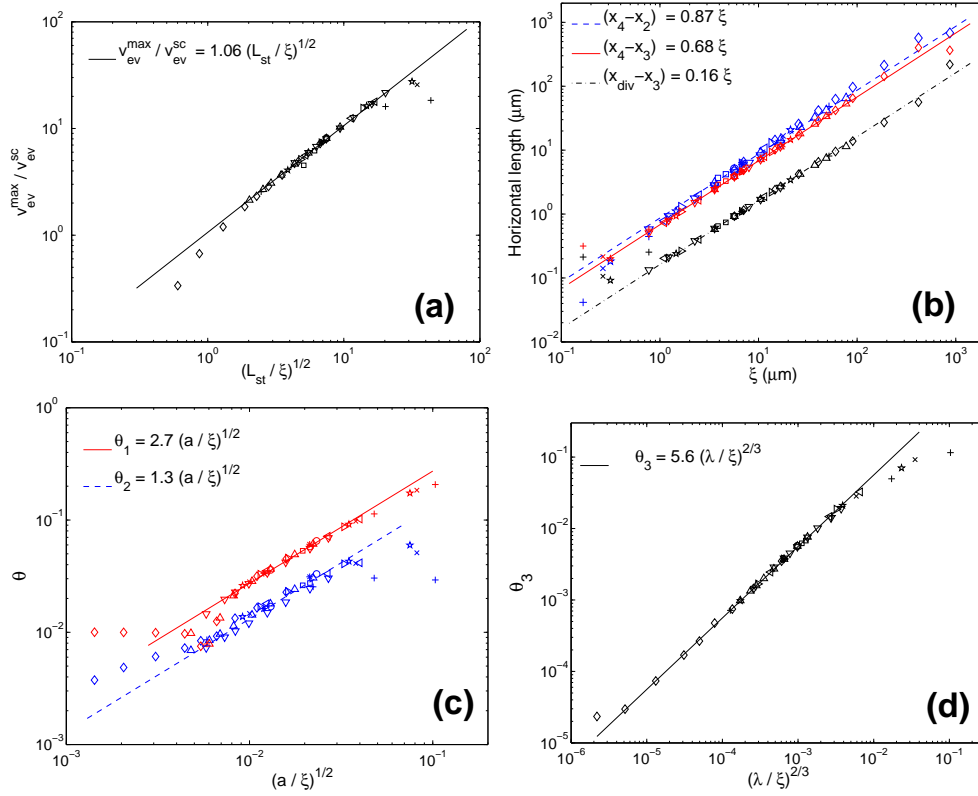


Fig. 2. Validation of scaling laws. Symbols : results from numerical simulations (see Table 2), lines : fit (see legend). (a) Maximum of evaporation velocity, (b) Horizontal lengths, (c) Local slopes at $x = x_1$ and $x = x_2$, (d) Local slope at $x = x_3$.

- Pham et al ([16] and erratum [17]) fix a priori the height of the film and a zero slope at the tip of the meniscus (corresponding to our $x = x_4$) where they impose a height which is equal to our expression of h_2 (while our numerical simulations give a very different thickness: $h(x_4) \sim 1\text{nm}$). The problem is solved by an approximated analytical method, validated by numerical simulations.

For both approaches, the estimation of the length of the precursor film (where disjoining pressure is non negligible) is found to be of order ξ , which is consistent with our result $(x_4 - x_2) \sim \xi$. Moreover, in the limit of zero contact line velocity (capillary number $Ca = 0$), these two models give the same scaling for the apparent contact angle:

$$\theta \sim \frac{(\eta \bar{v}_{ev})^{1/3} L^{1/6}}{A^{1/12} \sigma^{1/4}} \quad (20)$$

where θ is the contact angle, \bar{v}_{ev} is the mean evaporation rate, L is the droplet radius or the wedge size. It happens that this scaling is the same than the one we obtained for θ_1 or θ_2 (see Table 1). In addition, Pham et al find a prefactor equal to 2.5, which is very close to our value 2.7 for θ_1 (see figure 2c).

It is thus worthwhile to note that the three approaches lead to the same scaling for the macroscopic angle, while the description of the tip of the droplet or meniscus (for $x > x_3$) are very different. We suggest the following explanations:

- the squareroot profile of Deegan’s electrostatic analogy succeeds in giving the right integral of the evaporative flux outside the region where it falls down (i.e. for $x \lesssim x_3$).
- In all these models, there exists a domain of the droplet or the meniscus where fluxes corresponding to evaporation, capillary forces and Van der Waals forces are all of same order of magnitude. According to scaling analysis of section 3.3, this seems to be a key ingredient.

However models based on electrostatic analogy are not able to describe the end of the precursor film and it is necessary to shift to the complete model presented in this paper to get the film profile when the flux begins to decrease ($x > x_3$).

Finally, Eggers and Pismen [15] have studied the dynamic of evaporative drops retraction and have developed a model similar to the one presented in this study, taking into account explicitly the coupling between the liquid and the gas. They got the same scaling ξ for the width of the contact line region.

5 Conclusion

In this paper an hydrodynamic model has been developed to get a complete description of an evaporative meniscus in the configuration of complete wetting. The coupling between the liquid and gas is explicitly taken into account. Scaling laws based on heuristic arguments are derived for the different domains of the meniscus and validated by numerical simulations. Results are compared with previous models of the literature using the electrostatic analogy suggested by Deegan and co-authors. We show that the different approaches differ for the description of the tip of the meniscus in the domain corresponding to the decrease of the evaporative flux but lead to the same scalings for the apparent macroscopic contact angle. A possible extension should be to release the assumption of isothermal state [19].

Finally this model is based on a continuum description of the fluid. For the description of the tip of the meniscus, at the scale of the junction of the meniscus to the adsorbed film of nanometric thickness, the pertinence of such a model may be questionable. However this should have no effect on the estimation of the macroscopic apparent contact angle.

Acknowledgments

The authors gratefully acknowledge the financial support from the MULTIFLOW Marie Curie FP7-ITN Network and have benefited from fruitful discussions with H.Bodiguel, F.Lequeux, L.Limat and C. Pham. The numerical calculations have been performed on the computers of the "Direction des Services d’Information, Service Calcul" of the university UPMC.

References

1. D. Bonn, J. Eggers, J. Endekeu, J. Meunier, E. Rolley, *Reviews of Modern Physics*, **81**, (2009) 739-805
2. E. Rio, A. Daerr, F. Lequeux, L. Limat, *Langmuir* **22**, 22 (2006) 3186-3191
3. S.W. Hong, J. Xia, M. Byun, Q. Zou, Z. Lin, *Macromolecules* **40**, (2007) 2831-2836
4. H. Bodiguel, F. Doumenc, B. Guerrier, *Langmuir* **26**, 13 (2010) 10758-10763
5. A. Oron, S.H. Davis, S.G. Bankoff, *Reviews of Modern Physics*, **69**, 3 (1997) 931-980
6. C Sodtke, V.S. Ajaev, P. Stephan, *J. Fluid Mech.* **610**, (2008) 343-362
7. A. Rednikov, P. Colinet, *Microgravity Science and Technology*, **22**, 3 (2008) 249-255

8. G.T. Barnes, Adv. Colloid Interf. Sci., **25**, (1986) 89-200
9. C. Poulard, G. Guéna, A.M. Cazabat, Journal of Physics: Condensed Matter, **17**, (2005) S4213-S4227
10. C. Poulard, G. Guéna, A.M. Cazabat, A.Boudaoud, M. Ben Amar, Langmuir, **21**, (2005) 8226-8233
11. G. Guéna, P. Allançon, A.M. Cazabat, Colloids and Surfaces, **300**, (2007) 307-314
12. F. Doumenc, B. Guerrier, Langmuir **26**, 17 (2010) 13959-13967
13. R.D. Deegan, O. Bakajin, T.F. Dupont, G.Huber, S.R. Nagel, T.A. Witten, Nature **389**, (1997) 827-829
14. R.D. Deegan, O. Bakajin, T.F. Dupont, G.Huber, S.R. Nagel, T.A. Witten, Phys. Rev. E **62**, 1 (2000) 756-765
15. J. Eggers, L.M. Pismen, Physics of Fluids, **22**, (2010) 112101
16. C.T. Pham, G. Berteloot, F. Lequeux, L. Limat, EPL, **92** (2010) 54005
17. C.T. Pham, G. Berteloot, F. Lequeux, L. Limat, Erratum, EPL, **93** (2011) 54005
18. G. Jing, H. Bodiguel, F. Doumenc, E. Sultan, B. Guerrier, Langmuir **26**, 4 (2010) 2288-2293
19. S. Semenov, V.M. Starov, R.G. Rubio, M.G. Velarde, Colloids and Surfaces A **372** (2010) 127-134

A Scaling analysis

A.1 Maximum of evaporation velocity

We already established in section 3.2 that the evaporation flux decreases over a length:

$$(x_4 - x_3) \sim \xi \quad \text{with} \quad \xi \equiv \left(\frac{A}{\eta v_{ev}^{sc} \sqrt{L_{st}}} \right)^{2/3} \quad (\text{A.1})$$

We derive now the height h_3 and the angle θ_3 at $x = x_3$, where the evaporation flux reaches its maximum. In the region of decreasing evaporation flux, we must take into account the coupling between the liquid and the gas phases due to the effect of disjoining pressure on saturated vapor pressure (capillary pressure can be neglected in that region). After linearizing equation 10, we get the following scaling for the thickness:

$$h_3 \sim \left(\frac{\bar{v}_s A}{RT} \frac{c_{gs0}}{\Delta c_g} \right)^{1/3} \quad (\text{A.2})$$

with Δc_g the variation of vapor concentration in the gas phase above the liquid film, in the region of decreasing evaporation flux of characteristic length ξ . Assuming the same scaling for the horizontal and vertical components of concentration gradient ($\partial c_g / \partial x \sim \partial c_g / \partial z$), the boundary condition 9 gives a relation between Δc_g and v_{ev}^{max} :

$$D_g \frac{\Delta c_g}{\xi} \sim \rho v_{ev}^{max} \quad (\text{A.3})$$

Using equations A.2,A.3 along with 17 for v_{ev}^{max} , we get the desired scaling:

$$h_3 \sim \lambda^{2/3} \xi^{1/3} \quad \text{with} \quad \lambda \equiv \frac{\bar{v}_s}{RT} \sqrt{\eta P_{vs0} D_g} \quad (\text{A.4})$$

The angle θ_3 is then obtained by writing $\theta_3 \sim h_3 / \xi$.

A.2 Boundary between the bulk and the capillary zone

We see from numerical simulations that the slopes at $x = x_1$ and $x = x_2$ have the same scaling: $\theta_1 \sim \theta_2$. Let us denote $l_c \equiv (x_2 - x_1)$ the length of the capillary zone (liquid pressure dominated by the capillary term along with significant curvature gradient). The bulk region is characterized by a negligible curvature gradient, i.e. $\partial C/\partial x \ll C_0/l_c$. Therefore, at the boundary between bulk and capillary zones ($x = x_1$), we get the relation :

$$\frac{\partial C}{\partial x} \sim \frac{C_0}{l_c} \quad (\text{A.5})$$

Keeping the leading terms in equations 1 and 3, and assuming $l_c \gtrsim \xi$, we get:

$$\frac{\sigma}{\eta} h_1^3 \frac{\partial C}{\partial x} \sim J_0 \sqrt{l_c} \quad (\text{A.6})$$

Using equations A.5, A.6, 18 and relation $I(0) \sim I_w(0)$ to get J_0 , we obtain the following scalings:

$$l_c \sim a^{1/3} C_0^{-2/3} \quad \text{and} \quad h_1 \sim \theta_1 l_c \sim \frac{a^{5/6} C_0^{-2/3}}{\xi^{1/2}} \quad (\text{A.7})$$

Violation of condition $l_c \gtrsim \xi$ (i.e. $l_c \ll \xi$) corresponds to the transition to another regime, in which evaporation is negligible (see section 3.4).

B Numerical simulations : complementary results

We present in figure B.1 some results of numerical simulations to complete the validation of scaling laws presented in Table 1. The mean evaporation velocity is shown in figure B.1(a) (see equations 11 and 12 for the definition of \bar{v}_{ev} and v_{ev}^{sc} , respectively). Figures B.1(b-d) concern the liquid film thickness at each domain boundary. The prefactor resulting from the fit is indicated in each legend.

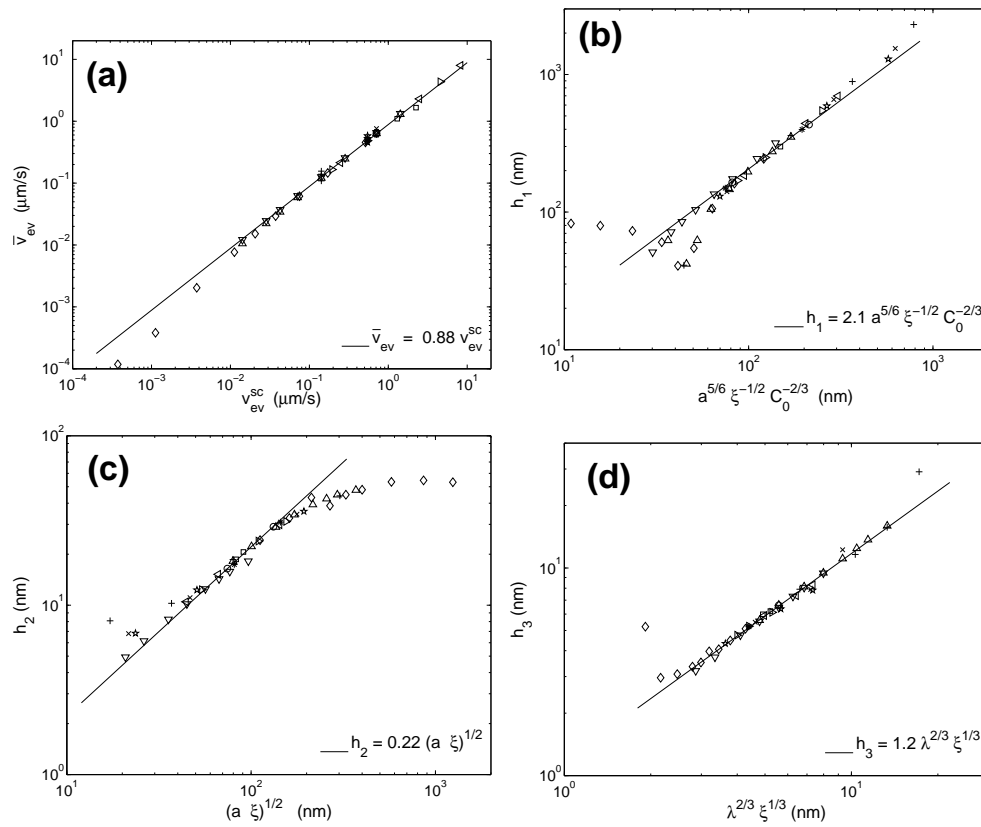


Fig. B.1. Validation of scaling laws. Symbols : results from numerical simulations (see Table 2), lines : fit (see legend). (a) Mean evaporation rate, (b) Film thickness at $x = x_1$, (c) Film thickness at $x = x_2$, (d) Film thickness at $x = x_3$.